HHS Public Access

Author manuscript

ACS Biomater Sci Eng. Author manuscript; available in PMC 2019 October 24.

Published in final edited form as:

ACS Biomater Sci Eng. 2019 February 11; 5(2): 959–969. doi:10.1021/acsbiomaterials.8b01331.

Development of an Injectable Nitric Oxide Releasing Poly(ethylene) Glycol-Fibrin Adhesive Hydrogel

Carly A Joseph, **Connor W McCarthy**, **Ariana G Tyo**, **Kenneth R Hubbard**, **Hannah C Fisher**, **Jacob A Altscheffel**, **Weilue He**, **Rattapol Pinnaratip**, **Yuan Liu**, **Bruce P Lee**, **Rupak M Rajachar***

Department of Biomedical Engineering, Michigan Technological University, Houghton, MI 49931

Abstract

Fibrin microparticles were incorporated into poly(ethylene) glycol (PEG)-fibrinogen hydrogels to create an injectable, composite that could serve as a wound healing support and vehicle to deliver therapeutic factors for tissue engineering. Nitric oxide (NO), a therapeutic agent in wound healing, was loaded into fibrin microparticles by blending S-Nitroso-N-acetyl penicillamine (SNAP) with a fibrinogen solution. The incorporation of microparticles affected swelling behavior and improved tissue adhesivity of composite hydrogels. Controlled NO release was induced via photolytic and thermal activation, and modulated by weight percent of particles incorporated. These NO-releasing composites were non-cytotoxic in culture. Cells maintained morphology, viability, and proliferative character. Fibrin microparticles loaded with SNAP and incorporated into a PEG-fibrinogen matrix, creates a novel injectable composite hydrogel that offers improved tissue adhesivity and inducible NO-release for use as a regenerative support for wound healing and tissue engineering applications.

Keywords

Fibrin Hydrogel; Inducible; Injectable; Microparticle; Nitric Oxide; PEG-NHS

1. Introduction

The minimally invasive nature of injectable hydrogels has made them a common therapeutic approach for wound repair and as regenerative supports for tissue engineering applications. Their capacity to serve as barriers to adhesion formations, act as a stable provisional matrix for cell attachment and load transfer, and broad potential for incorporating active elements (i.e. growth factors, protease inhibitors, platelets, and mesenchymal stem cells (MSCs)) to aid in wound healing has led to widespread interest for their use in soft tissue injury repair,

*Address for Correspondence: Rupak M Rajachar, Ph.D., 1400 Townsend Dr., Biomedical Engineering Department, Michigan Technological University, Houghton, MI, 4993 USA, Ph: (906) 487-1129, Fax: (906) 487-1717, rupakr@mtu.edu.

Supporting Information Available: The following files are available free of charge. Figure S1 shows characteristic UV-Vis absorbance spectra for SNAP before and after controlled degradation; Figure S2 provides UV-Vis abosorbance spectra showing SNAP stability is not affected by pH changes associated with microparticle synthesis; Figures S3–S5 provide H1-NMR spectra for SNAP and partially degraded SNAP incubated for 24 hours at 37°C and 60°C, and provides estimates for SNAP degradation with temperature; Figure S6 shows quantification of incorporated SNAP and the total quantity of NO released with SNAP loading in microparticles; Figure S7 shows FTIR analysis of microparticles and composite hydrogels.

including in ligaments and tendons. To that end and building on previous studies[1–2], this work addresses the challenge to create a tissue adhesive composite hydrogel that can serve as a preliminary matrix for soft tissue wound repair as well as a delivery vehicle for active molecules that support the wound healing process. Specifically, we have created a novel composite poly(ethylene) glycol-N-hydroxylsuccinimide (PEG-NHS)-fibrinogen adhesive hydrogel containing fibrin microparticles blended with the NO donor, S-nitroso-N-acetyl penicillamine (SNAP), to allow for the controlled release of nitric oxide as a wound healing support.

Fibrinogen exists physiologically as a 340 kDa glycoprotein, comprised of Aα (64kDa), Bβ (57 kDa), and γ (48 kDa) subunits bound by disulfide linkages[3–4]. Fibrinogen hydrogels are unique compared to other polymers due to their nonlinear fiber architecture consisting of thin protofibrils and thick fibers, creating the capacity to respond to mechanical loads at multiple length scales[5]. Additionally, these materials can be cross-linked to control stability and degradation behavior, i.e. hydrolysis of PEG-linkages to fibrinogen or fibrinogen to itself[6]. Fibrinogen-based hydrogel materials have been shown to inherently facilitate cell adhesion and promote regeneration through enhanced angiogenesis and cell viability[7]. Fibrinogen is part of the provisional extracellular matrix (ECM) during tissue repair, and is already a clinically established matrix for wound healing treatment[8,9]. Not only does it directly attract and bind different cell types, but fibrinogen also has the ability to bind growth factors from the platelet-derived growth factor (PDGF), fibroblast growth factor (FGF), and transforming growth factor (TGF-β) families, which are known regulators of tissue remodeling, properties which in turn can aid in degrading a PEG-fibrinogen hydrogel over time and in replacing the hydrogel with ECM[8,4, 10].

Nitric oxide (NO) plays a significant role in tissue turnover and wound healing and has been implicated as a necessary factor in various wound-injury healing conditions including tendinopathy[11–12]. The beneficial effects of NO in specific tissues and under physiological conditions is tightly bound to its controlled availability, a result of its limited half-life and its spatial and temporal expression. Recent work has revealed that exogenously generated NO has therapeutic potential for the treatment of infection[13] and modulation of wound healing[14], in addition to its already established role in vascular perfusion and angiogenesis[15]. More specifically, several trends are becoming increasingly clear regarding the role of NO in a reparative microenvironment and its tissue-specific availability. At low concentrations, NO tends to have an anabolic effect on tissues. For example, within injured tendon (i.e. Achilles and supraspinatus), there is an elevated NO activity that is expressed in fibroblast-like cells (tenocytes) that peaks at seven days post injury. Further, inhibition of NO production during tendon repair results in a significant reduction in stable reparative tissue volume[16]. Conversely, at higher concentrations NO tends to promote catabolic activities or results in a quiescence of regenerative activity[17–18]. These seemingly conflicting tissue responses to NO may in part be caused by matrix metalloproteinases (MMPs), which can be either activated or inactivated by NO depending on its concentration and timing[19]. Thus, if not tightly controlled, elevated or depressed NO availability can lead to potentially detrimental effects including apoptosis, loss of tissue stability, and structural atrophy[20–21].

Although recent work has shown the efficacy of NO therapy (i.e. injected and topical NO-donor group delivery) on soft tissue healing and regeneration[11, 16], evidence regarding the time-dependent mechanisms by which NO impacts wound repair at a matrix level (i.e. MMP regulation) suggests these transient unregulated approaches may potentially lead to long-term loss of tissue architecture and ultimately function if NO is not targeted and controlled. However, to date, practical, inducible NO-release systems remain limited[22–23]. Recent work regarding tenocyte activity suggests a concentration window for therapeutic outcomes including stable fibroblast proliferation and matrix synthesis[16, 20]. What is needed are easily deployed materials (injectable) that contain either NO or an inducible NO precursor that can release NO in a controlled and appropriately sustained manner.

S-nitrosothiols (RSNOs) are capable of donating NO under favorable conditions through the cleavage of the covalent S-N bond, liberating nitric oxide (NO•) and a thiyl radical (RS•)[24]. The well-known NO donor, S-nitroso-N-acetyl penicillamine (SNAP), has been used to release NO through photolytic cleavage of the S-N bond[25]. For use in clinical applications, recent studies have demonstrated the potential for NO release through compressive and shear mechanisms in addition to thermal mediated pathways, presenting a more clinically relevant and viable option for the application of site specific controlled NO release[1].

In this work, we describe the novel synthesis of inducible, NO releasing fibrin microparticles and the creation of a microparticle incorporated, 4-arm PEG-NHS-fibrinogen composite adhesive hydrogel. First, we fabricated and characterized fibrin microparticles and then blended SNAP into fibrin microparticles and verified controlled NO release. Next, we incorporated microparticles into a PEGNHS-fibrinogen matrix. PEG-NHS is a primary amine ($-NH_2$) reactive PEG derivative that can be used to crosslink with fibrinogen, fibrin microparticles, and tissue at a wound site. We then characterized the nitric oxide release behavior as well as the physical, rheometric, and adhesive properties of the composite hydrogels. Last, we assessed the effect of these composite hydrogels on cell viability. To the authors knowledge the composite hydrogels developed in this work are the first injectable delivery vehicle capable of acting as a suitable scaffolding for repair that is also tunable for releasing NO at controlled levels to promote the anabolic effects of NO as a site-specific donor. The advantages of an injectable delivery system are twofold; the material is able to conform to the local microenvironment and make use of an inherent adhesive character to physically integrate within the injury site. Adhesion is achieved through the formation of interfacial covalent bonds created between 4-arm PEG-NHS and amine and thiol groups found in tissue ECM in addition to the inherent adhesive qualities provided by fibrinogen/fibrin matrix components[26–30].

2. Materials & Methods

2.1. Synthesis and characterization of S-Nitroso-N-acetyl penicillamine (SNAP)

SNAP was synthesized using a previously published protocol[31–33]. Briefly, N-acetyl-D-penicillamine (NAP), hydrochloric acid, methanol, and sulfuric acid were obtained from Sigma Aldrich (St. Louis, MO). Sodium nitrite (99.999% metals basis) was purchased from Alfa Aesar (Ward Hill, MA). 1000 mg of NAP was sonicated in 25 mL of methanol. Once dissolved, 15 mL of 1M HCl and 500 μL concentrated H_2SO_4 were added. Then, 724.5 mg

of sodium nitrite was added to this solution and mixed until all solids had dissolved. The solution was allowed to react for one hour, developing a dark green color, and then cooled in an ice bath for 45 minutes. Methanol was removed by rotary evaporation, yielding a dark green, crystalline product. Crystals were ice cooled and isolated by vacuum filtration in deionized water, followed by an additional vacuum step to ensure all solvents had been eliminated. Both Ultraviolet-visible light spectroscopy (UV-Vis) and ^{1}H nuclear magnetic resonance (NMR) were used to confirm synthesis of SNAP product and also verify that pH and temperature changes used in composite synthesis did not significantly degrade SNAP product. For UV-Vis, 0.33 mg/ml of SNAP was dissolved in methanol. A Perkins Elmer's UV-Visible spectrometer was used to detect the absorbance of SNAP in solution from 600 nm to 290 nm. Peak absorbance of SNAP is at 340 nm (Figure S1–S2). For NMR, 4 mg/ml of SNAP was dissolved in DMSO-D_6. NMR was used to detect protons in the solution. Shifts in peak position were observed and correlated to the known chemical structure of the sample (–CH_3 at 1.84,1.91, and 1.93, -NH at 8.47, and -CH at 5.13 with integration ratio of 3:3:3:1:1) and their degraded product (-CH_3 at 1.85, 1.25, and 1.29, -NH at 8.09, and –CH at 4.34). Integration of peak area was used to confirm the proton ratio of the sample (Figure S3–S5).

2.2. Synthesis of SNAP-Fibrinogen

Phosphate buffered saline (PBS) was obtained from Calbiochem (San Diego, CA). Sodium hydroxide, fibrinogen (from bovine plasma, > 75% clottable protein), and acetone were obtained from Sigma Aldrich (St. Louis, MO). In preparation for microparticle fabrication, SNAP (20 mg) crystals were combined with 1.8 mL of phosphate buffered saline at a pH of 7.4. To fully dissolve the SNAP, the pH was briefly adjusted to 10.5 through the dropwise addition of 1M NaOH. The solution was then immediately adjusted to a pH of 5.5 through the addition of 1M HCl. Fibrinogen (200 mg) was then added to SNAP solution, and was placed on a shaker table until the fibrinogen had fully dissolved.

2.3. Microparticle Fabrication

Two types of microparticles, fibrin and SNAP-fibrin, were generated. Calcium chloride was purchased from Fisher Scientific (Waltham, MA). Thrombin (from bovine plasma) was purchased from Akron Biotech (Boca Raton, FL). The fibrinogen or SNAP-fibrinogen solution was added dropwise with a syringe using a 27-gauge needle (Beckton Dickinson; Franklin Lakes, NJ) to 75 mL of stirring olive oil (Great Value; Bentonville AR) heated to 60°C. Inverse emulsions were prepared at stirring speeds of 750, 1000, and 1500 rpm in a 250 mL round bottom flask, using an overhead stirrer (Fisher Scientific D25; Waltham, MA) and a 2-blade Teflon impeller (Fisher Scientific; Waltham, MA). Particles generated at rotation speeds of 750, 1000, and 1500 rpm were designated as R1, R2, and R3 particles, respectively. Particles made with fibrinogen only are referred to as R1, R2, and R3. Particles made with SNAP-fibrinogen are referred to as R1-SNAP, R2-SNAP, and R3-SNAP. Immediately following the addition of the fibrinogen or SNAP-fibrinogen solution, 50 units of thrombin with 3 mg of $CaCl_2$ in 0.5 mL of PBS was added dropwise to the flask and allowed to stir for 10 minutes. The heated water bath was then exchanged for an ice bath and allowed to stir for an additional 10 minutes. The stirring speed was subsequently reduced to 500 rpm and 25 mL of chilled acetone was added to the flask. The emulsion was stirred for

two additional minutes, after which the particles were isolated by vacuum filtration, rinsed with chilled acetone to remove residual oil, and vacuum dried for one hour. Particles were stored at −20°C for later use.

2.4. Field Emission Scanning Electron Microscopy and Microparticle Analysis

In preparation for imaging, microparticles were vacuum dried and homogenized, then mounted to conductive carbon tape. A Hummer 6.2 Sputter coater (Anatech, Ltd; Battle Creek, MI) was used to deposit 5 nm of Au/Pd on the surface of samples. Samples were imaged with an accelerating voltage between 3–5 kV and a beam current of 8 μA on a Hitachi S4700 field emission scanning electron microscope (Schaumburg, IL).

Particle analysis was performed using NIH ImageJ software. Images were manually analyzed to determine average particle diameter and distribution for R1, R2, and R3 particle preparations. Three images per preparation were analyzed from three independent batches of particles. A grid system (0.37 mm^2 × 24) was superimposed over each image, creating 24 squares available for analysis. A random number generator was used to select 4–5 squares per image, and all discernable particles in those grids were measured.

A gamma distribution function (Equation 1) describing a probability density with parameters α, the shape parameter, and β, the scale or rate parameter was used to describe each particle size distribution. The gamma distribution incorporates the gamma function, shown in Equation 2. The α parameter must be a positive scalar value, while β must be a non-negative scalar[34].

$$f(x;\alpha,\beta)=\frac{1}{\beta^{\alpha}\Gamma(\alpha)}x^{\alpha-1}e^{-x/\beta} \quad (1)$$

$$\Gamma(k)=\int_0^{\infty}x^{k-1}e^{-x}dx, \quad k\in(0,\infty) \quad (2)$$

The diameters of the particles collected were allocated into 125 evenly distributed bins and a histogram plot of frequency versus the particle diameter was generated. Then, a gamma distribution was fit to the data, where 95% ($p \le 0.05$) confidence intervals were calculated for the parameters α and β.

2.5. Nitric Oxide Release from Microparticles

Nitric oxide release was evaluated in real-time through chemiluminescent analysis with a Sievers 280i nitric oxide analyzer (NOA; Boulder, CO). Fibrin microparticles were weighed (5 mg) and placed into a dry reaction cell for analysis. Samples were swept with dry, nitrogen gas and irradiated with a 470 nm LED (VAOL-5GSBY4; VCC Optoelectronics; San Diego, CA) attached to the sample vial to promote NO release. Chemiluminescent NO release was induced in a stair step fashion from 0.4 volts to 1 volt (0.4V, 0.6V, 0.8V, 1V, 0.8V, 0.6V, 0.4V) for 5 minutes at each voltage using the LED. The LED was turned off for 5 minutes between each change in voltage. The resulting data was normalized to sample mass. Nitric oxide depletion was also determined at two particle weights (4mg and 8mg) to assess for total NO content (Figure S6).

2.6. Microparticle Incorporation into PEG-Fibrinogen Hydrogels

Four-arm polyethylene glycol succinimidyl glutarate (PEG-NHS) was obtained from JenKem Technologies (Plano, TX). Fibrinogen (Fgn) from bovine plasma and PBS were purchased from Sigma Aldrich (St. Louis, MO). PEG-NHS (67 mg/mL) and fibrinogen (134 mg/mL) were dissolved separately in PBS (pH 7.4). Previously generated R2-microparticles were added to the PEG-NHS solution (5.9 wt % R2-SNAP microparticles). The dissolved components were mixed at a PEG-NHS:fibrinogen ratio of 1:2 (w/w) in a glass vial by vortexing for 10 seconds and pipetted immediately into cylindrical polytetrafluoroethylene molds (12 mm diameter), where they were allowed to fully cure. Alternately, PEG-NHS and fibrinogen solutions could be mixed using a dual barrel syringe (Practicon; Greenville, NC). The gelation character was evaluated using a standard tip test. R2 microparticles were used in all composite hydrogel formulations. Composite hydrogels containing the fibrin-only microparticles were defined as PEG-NHS-Fgn-R2. Composite hydrogels containing the SNAP-fibrin microparticles were defined as PEG-NHS-Fgn-R2-SNAP. The microparticle-free PEG-NHS-fibrinogen hydrogels served as controls for all experiments, and were defined as PEG-NHS-Fgn. Fourier transform infrared (FTIR) spectra were obtained for particle and hydrogel samples. Briefly, samples were equilibrated in PBS (pH = 7.4) and dried under vacuum for 2 days and all measurements were made using a PerkinElmer Spectrum One Spectometer (Figure S7).

2.7. Nitric Oxide Release from Composite Hydrogels

Nitric oxide release was induced using photolytic cleavage and thermal activation in separate experiments. PEG-NHS-Fgn-R2-SNAP hydrogel composites (12mm diameter, 7mm height) of three distinct microparticle weight percent (1.8%, 3.6%, and 5.9%) were evaluated for NO release character. For chemiluminescent analysis, gel samples were placed into a sample vial and a 470 nm LED was used to promote release of NO at 22°C, and cumulative NO release in ppb was determined. In thermally induced NO release, samples were evaluated at 22°C, 37°C, and 40°C for 1 hour per sample, and NO flux (mol/min·cm^2) was recorded. Flux measurements were chosen in lieu of cumulative release measurements to account for the period required for temperature equilibration between samples. An average of three measurements were made for each sample per temperature, and results were normalized to sample volume.

2.8. Swelling Behavior, Water Content, & Degradation

The swelling behavior of the 5.9wt% PEG-NHS-Fgn-R2 hydrogel composites and PEG-NHS-Fgn control hydrogels was determined by hydrating samples in PBS at a pH of 7.4 for 16 hours. Samples were individually blotted to remove surface fluid, and weighed to determine the hydrated mass (W_H). Samples were then placed under vacuum for 12 hours to remove all water content from the gels, and weighed again to determine the dehydrated mass of the sample (W_D). The swelling ratio (W_S) and water content (WC) of the gels were determined as follows (Equations 3 and 4):

$$W_S = \frac{W_H}{W_D} \tag{3}$$

$$WC = \frac{W_H - W_D}{W_H} \tag{4}$$

To assess degradation behavior, control PEG-NHS-Fgn hydrogels and 5.9wt% PEG-NHS-Fgn-R2 hydrogel composites were prepared as previously described. Samples were individually placed in PBS at a pH of 7.4. Samples were stored at 37°C and 5% CO_2, and were visually monitored until complete dissolution (hydrogel completely solubilized).

2.9. Rheological Characterization

An HR-2 rheometer (TA Instruments; Newcastle, DE) equipped with a Peltier hood to prevent dehydration of gels during testing was used to determine the rheological character of the hydrogel composites. The parallel plate diameter was 20 mm, with a plate separation of 90% of the gel thickness. Frequency sweep experiments (between 0.1 Hz and 100 Hz, with 5 measurement points per decade) were conducted on 5.9wt% PEG-NHS-Fgn-R2 hydrogel composites and PEG-NHS-Fgn control hydrogels. Samples were evaluated at 10% strain in compression and 1% strain in shear. Storage modulus (G') and loss modulus (G'') were determined.

2.10 Lap Shear Adhesion Testing

Adhesive properties of PEG-NHS-Fgn control, 3.6wt% PEG-NHS-Fgn-R2 hydrogel composites, and 3.6wt% PEG-NHS-Fgn-R2-SNAP hydrogel composites were tested according to the American Society for Testing and Materials (ASTM) standard F2255–05[35]. Briefly, 120 μL of hydrogel solution (prepared as previously described) was added onto the overlap area of two pieces of bovine pericardium and cured in situ with an overlap area of

2.5cm × 1cm. A 100g mass was applied to the overlapping area for 10 minutes. Samples were then placed in PBS and stored at room temperature overnight. The adhesive area of each sample was measured before lap shear testing. Samples were loaded in shear at a rate of 5mm/min until complete separation. The adhesive strength was obtained by dividing the max load by the adhesive area measured prior to testing.

2.11 Live/Dead Viability Assay

Cytotoxicity was first measured using live-dead fluorescence imaging. PEG-NHS-Fgn-R2-SNAP composite (3.6 wt%) and PEG-NHS-Fgn control hydrogels were sterilized in 70% ethanol followed by rinsing in sterile PBS. Hydrogels were then seeded and cultured with L929 fibroblasts (ATCC) (7.7×10^4 cells/cm^2) in Dulbecco's modified Eagle's medium (DMEM) containing 10% fetal bovine serum (FBS) and 0.5% penicillin-streptomycin at 37°C and 5%CO_2 for 48 hours. Cell viability was evaluated by staining with calcein-AM (live) and ethidium bromide (dead), followed by fluorescence imaging and assessment for the presence of live and dead cells. Cell counts were performed using ImageJ software (NIH, Bethesda, MD).

2.12 MTT Proliferation Assay

To assess cell proliferation behavior, an MTT proliferation assay (Sigma Aldrich) was used with extracts from 3.6 wt% PEG-NHS-Fgn-R2-SNAP hydrogel composites and PEG-NHS-Fgn controls incubated for 24 hours in DMEM at culture conditions. The MTT Cell Proliferation Assay measures the cell proliferation rate, when changes in cellular metabolism lead to apoptosis or necrosis, this results in a reduction in cell viability. L929 fibroblasts were seeded with conditioned media containing 100uL of extracts in 96-well plates at a density of 1×10^4 cells/well. Cells cultured in DMEM served as controls. After 24 hours, the media from each well was replaced with 50uL of MTT solution (1 mg/mL in PBS) and plates were incubated for an additional 2 hours. The MTT solution was exchanged for 100uL isopropanol/well and the absorbance of each well was measured at 570 nm (reference 650 nm) using a Synergy HT Multi-Mode Microplate Reader (BioTek, USA). The relative cell viability was determined as follows (Equation 5):

$$\%\ cell\ viability = \frac{\mathrm{Abs}_{\mathrm{hydrogel}}}{\mathrm{Abs}_{\mathrm{control}}} \times 100 \quad (5)$$

where $\mathrm{Abs}_{\mathrm{hydrogel}}$ and $\mathrm{Abs}_{\mathrm{control}}$ are the absorbance for cells cultured in hydrogel media extracts and standard media, respectively. Four independent cultures were prepared for hydrogel composites and control hydrogels. Samples with relative cell viabilities greater than 70% were considered non-cytotoxic.

2.12 Statistical Analyses

All experiments were performed in triplicate (n = 3) unless otherwise stated. For quantitative analysis, comparisons were made using ANOVA with a standard t test, with p-values ≤ 0.05 considered significant. Error bars represent standard error of the mean unless otherwise stated.

3. Results and Discussion

3.1. Microparticle Fabrication & Analysis

Typical emulsion polymerization is used to polymerize relatively water-insoluble monomers[36]. In this case, we used an inverse emulsion polymerization process in which water soluble monomer and initiator are added to oil to create an emulsion polymerization system[37]. Fibrin microparticles were fabricated in this way by forming an emulsion through fluid shear force generated by stirring (Figure 1).

Fibrin particles were imaged using scanning electron microscopy, and were characterized by the average particle diameter and particle size distribution by fitting that data to a distribution equation (Figure 2). Representative images of particle morphology for three stirring conditions are shown in Figure 3A–C. The mean particle diameters ranged from 78–193 μm. Morphologically, the R1 samples were characterized by excessive debris and irregularly shaped particles (Figure 3A). R2 samples exhibited little debris, with spherical particles and a much narrower size distribution (Figure 3B). R3 particles were shown to have the smallest mean diameters and the narrowest size distribution, however these particles were also characterized by the presence of excessive debris and particle irregularity (Figure 3C). The approach used to generate microparticles in this work was similar to that of other studies, and we observed a characteristic decrease in particle size and narrowing of the size distribution as seen in other systems[38–39]. However, the unique polymerization process of fibrinogen in the presence of thrombin may explain some of the observations regarding the heterogeneity (i.e. presence of debris and irregular particle morphology) created in particle distributions with varying rotational speeds. Specifically, elevated shear may differentially affect formation of stable particle morphologies at the level of monomer unfolding, formation of protofibrils and protofibril bundles, as well as at the fiber level[5]. Based on the data and images gathered from this analysis, for this particular work, R2 particles were chosen for incorporation into the composite hydrogels for their uniformity, lack of debris, and relatively narrow distribution.

3.2. Nitric Oxide Release from Microparticles

NO release from the microparticles was evaluated to confirm the stable incorporation of SNAP within the particles. NOA measurements showed that all particle formulations had the capacity to release measurable amounts of NO and that this release behavior could be actively controlled using an external energy source. Using an LED, photolytic NO release was induced and recorded as average release for each particle size group and normalized to mass (Figure 4). As would be expected with any surface release phenomenon, the average release appears to be affected by the available surface area, with average release based on particle sizes of 1.01 ± 0.74 ppb, 6.12 ± 3.19 ppb, and 5.67 ± 2.13 ppb for R1, R2, and R3

particles respectively. Thus, R1 particles as expected have a very low average release compared to R2 and R3. Variabilities described in the quality of R3 particles may explain why the average release behavior is indistinguishable between R2 and R3 formulations.

3.3. Microparticle Incorporation into PEG-Fibrinogen Hydrogels

Composite hydrogels were made by incorporating microparticles into a base PEG-NHS-Fgn hydrogel (Figure 5). The PEG-NHS-Fgn-R2 hydrogel composites contained the fibrin-only microparticles, and the PEG-NHS-Fgn-R2-SNAP contained the NO releasing SNAP-fibrin microparticles. The fully injectable system was deliverable using a dual-barrel mixing syringe. Microparticles were intact and dispersed throughout the hydrogel structure. The curing-time for all formulations was 46.7 ± 2.4 seconds, as measured using a simple tip test. The relative ease at which NO releasing SNAP-fibrin microparticles can be incorporated into the base PEG-Fgn matrix makes it a practical approach to create an injectable hydrogel with tailored NO release properties.

Previous studies from our group showed that primary amines on fibrin based hydrogels could be covalently modified with SNAP to create inducible NO-releasing scaffolds[1] and that PEG-NHS-fibrinogen composites could also be modified post-gelation to create composite inducible NO-releasing scaffolds[2]. The direct-derivatization of fibrinogen to form SNAP-fibrinogen results in a dramatic loss of solubility in aqueous solutions precluding their use in generating reproducible gelation kinetics and hydrogel properties. Incorporating SNAP-fibrin microparticles into the PEG-Fgn matrix reduces the time required to prepare a NO-releasing hydrogel, and has also proven to be more reproducible than approaches using direct-derivatization of fibrinogen.

3.4. Nitric Oxide Release from Hydrogel Composites

NO release from PEG-NHS-Fgn-R2-SNAP hydrogel composites was evaluated to ensure that there was no release inhibition once the microparticles were incorporated into the hydrogel. Cumulative NO release (ppb) was measured via photolytic (light) activation (Figure 6A) and NO flux (mol/min·cm^2) was measured via thermal activation (Figure 6B). In general, release behavior was tunable with a unique activation profile for each mechanism, photolytic and thermal activation respectively.

More specifically, at the lowest microparticle content (1.8wt%), the average NO release induced by photolytic activation was 7.76 ppb ±2.24. With increasing microparticle content (3.6 wt% and 5.9wt%), the average release was 135 ± 25.1 ppb and 242 ± 31.0 ppb, respectively. These results indicated that photolytic induced NO release was dependent on microparticle loading in composite hydrogels.

Thermally induced NO release was also measured for 5.9 wt% PEG-NHS-Fgn-R2-SNAP hydrogel composite samples at three distinct yet clinically relevant temperatures: room temperature (22°C), body temperature (37°C), and the clinical limit for injury treatment using direct heat application (40°C). NO flux values were $7.08 \times 10^{-12} \pm 1.73 \times 10^{-12}$, $1.56 \times 10^{-11} \pm 1.31 \times 10^{-12}$ and $2.05 \times 10^{-11} \pm 1.80 \times 10^{-13}$ mol/min·cm^2 for 22°C, 37°C, 40°C groups respectively. Each increase in temperature yielded significant increases in NO release, which is consistent with results from our previous work[1], and this magnitude of NO

flux is broadly consistent with other NO releasing systems designed for biomedical applications[40–44].

These results indicate the feasibility of using equilibrated heating and cooling cycles within a clinically acceptable range to control local delivery of NO to injured tissue. NO has been shown to modulate multiple signaling pathways relevant in wound healing, but the challenge of promoting only its beneficial effects hinges on controlling its concentration and temporal release profile *in vivo*. For example, NO signaling can alter the M1/M2 macrophage balance, promote angiogenesis via activation of HIF-1α and VEGF, and can cause both activation and inhibition of matrix metalloproteinases (MMPs) depending on its concentration and timing[19, 45–46]. To this end, creating a means of NO delivery that could be activated at specific time points after the initial injection of the hydrogel is of significant clinical relevance.

Other NO releasing biomaterials have shown promising results in skin wound healing[47] and cardiovascular applications such as the therapeutic delivery of mesenchymal stem cells for the treatment of myocardial infarction[48], but are either precast or dependent on enzymatic activity *in situ* for NO release. To our knowledge, this is the first injectable composite NO delivery system that would allow temporal control of release at the injury site. The exact range of NO flux desired for this particular application is not known, but the tunable NO release character of this material, based on the amount of SNAP-fibrin (R2-SNAP) microparticles incorporated as well as controlled thermal activation, makes it amenable for targeting a tissue specific level of NO flux. In the context of tendon repair, a useful application of temporal control of NO delivery would be the ability to control MMP activation and inhibition. MMPs are enzymes that digest collagen, gelatin, and other structural molecules and are critical in normal ECM homeostasis, but increased and prolonged MMP activation has been shown to potentiate ECM dysregulation and tendon injury[49].

3.5. Swelling Behavior, Water Content, & Degradation

The PEG-NHS-Fgn-R2 hydrogel composites were found to have significantly lower swelling and water content compared to PEG-NHS-Fgn controls (Figure 7A). Incorporation of fibrin microparticles and/or greater crosslinking between the matrix components could explain the exclusion of water observed in hydrogel composites.

Degradation time, as indicated by the number of days before the complete dissolution hydrogels, was statistically indistinguishable between control hydrogels and hydrogel composites. Degradation times ranged from 29.5 ± 1.00 (control) to 31.6 ± 3.77 (hydrogel composites) days. The temporal presence of these hydrogels mirrors an expected wound healing response timeline. For example, in tendon wound healing, the hemostasis and inflammation phase takes place over days, the proliferation and fibroplasia phase occurs over several weeks, and the remodeling phase where the tissue strength approaches that of uninjured tissue occurs after months[50]. Given that both the PEG-NHS-Fgn control hydrogels and the PEG-NHS-Fgn-R2 hydrogel composites maintained structural stability for approximately 30 days, these composites may be tailored for differential load transfer within this window from the hydrogel matrix to the healing tissue at a physiologically appropriate

time point. A more specific understanding of the effect of microparticle content on the mechanical properties and degradation behavior of the composite hydrogel warrants further study. Controlling the swelling behavior and degradation properties will allow the composite hydrogel system to be tuned to the specific injury site and application.

3.6. Rheological Characterization

Oscillatory rheometry testing was used to determine the viscoelastic (time-dependent) behavior of PEG-NHS-Fgn-R2 composite hydrogels compared to PEG-NHS-Fgn controls, where the elastic character is represented by the storage modulus (G') and the viscous character by the loss modulus (G") (Figure 7B). The storage modulus (G') was significantly higher than the loss modulus (G") for both controls and composites, indicating that the hydrogels were chemically crosslinked. The stiffness of PEG-NHS-Fgn control and PEG-NHS-Fgn-R2 composite hydrogels as measured by G' did not vary significantly with frequency. This may be the result of several phenomenon including variations in the nature and level of cross-linked units (i.e. PEG-fibrinogen-PEG; PEG-fibrin microparticle-PEG; fibrinogen-PEG-fibrinogen) as well as differences in the water swelling character of composite hydrogel and component fibrin microparticles. The G" increased with frequency with the addition of fibrin microparticles. The elevated G" suggests an increased viscous dissipation ability of the composite hydrogel[51]. The reversible physical bonds (weak interactions, i.e. chain entanglements, van der Waals forces, electrostatic forces) existing in the composite structure can be sacrificed before the breaking of chemical bond during energy dissipation, suggesting on average these composites are slightly more viscous in character compared to controls at lower loading frequencies.

3.7 Lap Shear Adhesion Testing

Soft tissue injuries, such as tendinopathies, often result due to a failure of the tissue to adapt to mechanical loading. Thus, creating an adhesive scaffold is important because it should allow for the stable transfer of loads between the scaffold and underlying tissue, facilitating cellular infiltration and stable growth with appropriate mechanical cues. All tested hydrogel formulations are inherently tissue-adhesive materials as PEG-NHS reacts with the amine and thiol groups of proteins present in tissue to form amide bonds and covalent adhesion to tissue[30, 52]. PEG-NHS-Fgn-R2 and PEG-NHS-Fgn-R2-SNAP hydrogel composites exhibited significantly increased adhesive character compared to PEG-NHS-Fgn controls, indicated by a 1.5-fold and 3-fold increase in adhesive strength respectively (Figure 8). This increase can be attributed to a reinforcement of the PEG-NHS-Fgn matrix provided by the presence of the microparticles. Other composite PEG hydrogels, such as gelatin microgels in a PEG matrix, exhibit similar behavior[36]. Furthermore, a unique and interesting finding of this particular work was that PEGNHS-Fgn-R2-SNAP composites showed significantly higher adhesive strength over both controls and fibrin-only composites, indicating that NO release has the potential to improve adhesive properties. During testing, it was noted that samples failed internally rather than at the gel-tissue interface. Since failure of these hydrogels occurs through an intra-molecular mechanism (cohesive forces as opposed to adhesive forces), there is potential to increase the adhesive strength even further with the addition of more microparticles or by increasing intramolecular crosslinking via another method.

3.8 Live/Dead Viability Assay

Live/dead analysis showed the presence of viable fibroblasts both on PEG-NHS-Fgn control and PEG-NHS-Fgn-R2- SNAP hydrogel composite cultures. Cells are able to directly bind to fibrinogen/fibrin through integrins, and fibroblasts specifically are able to adhere at the Arg-Gly-Asp (RGD) sequence on the C-terminal Aα chain of fibrinogen/fibrin through $\alpha_v\beta_3$ integrins[4]. Cells in both cultures were adherent and showed no significant differences in viability indicated by calcein staining (>90% survival for all cultures). All cultures remained viable for at least 2 days following initial seeding, in addition to these results, qualitative assessment of morphological character showed that cells seeded on the hydrogels show good adherence and spreading, indistinguishable from controls (Figure 9A–B).

3.8 MTT Proliferation Assay

Complementary MTT proliferation data reinforces the live/dead results by showing that cells seeded on PEG-NHS-Fgn-R2-SNAP hydrogel composites retain their proliferative character indicative of a microenvironment suitable for normal cell behavior. Relative cell viability above 70% indicates gels are non-cytotoxic to cultured cells. Both the PEG-NHS-Fgn-R2-SNAP hydrogel composites and the PEG-NHS-Fgn control hydrogels met this condition, with relative cell viabilities of 91.7 ± 15.3% and 98.3 ± 13.9% respectively (Figure 9C). Although it is known that the MTT assay is susceptible to thiol species, live/dead assay data corroborate the MTT results (>90% cell viability where the cut-off for cytotoxicity is set at 70%).

4. Conclusion

This work presents a novel method to incorporate NO release into an injectable, biocompatible adhesive composite hydrogel for use in soft tissue wound healing applications. Spherical fibrin microparticles can be synthesized using inverse emulsion polymerization, and NO release can be achieved through the addition of SNAP. These particles can be easily incorporated into a PEG-fibrinogen hydrogel at a chosen weight percent. The fibrin microparticles served as a robust delivery vehicle, where controlled NO release could be induced via photolytic and thermal activation. Microparticle incorporation into the PEG-fibrinogen matrix to create composite hydrogels also revealed distinct changes in physical properties, including decreased swelling ratio and increased adhesive character. These injectable composites exhibited excellent biocompatibility *in vitro*, and will be the basis of future *in vivo* studies. Future work will also explore the mechanisms involved in the improved adhesive property of the NO releasing composites, as well as the potential ability of the NO releasing composite hydrogel to control MMP activity to facilitate improved tendon repair.

Supplementary Material

Refer to Web version on PubMed Central for supplementary material.

Acknowledgements

The authors would like to thank Dr. Megan Frost at MTU for the training and use of the NO analyzer. This work was supported by the National Institutes of Health under Award Numbers R15GM112082 (RMR) and R15GM104846 (BPL).

References

1. VanWagner M; Rhadigan J; Lancina M; Lebovsky A; Romanowicz G; Holmes H; Brunette MA; Snyder KL; Bostwick M; Lee BP, S-nitroso-N-acetylpenicillamine (SNAP) derivatization of peptide primary amines to create inducible nitric oxide donor biomaterials. ACS applied materials & interfaces 2013, 5 (17), 8430–8439.10.1021/am4017945. [PubMed: 23964741]
2. Brunette M; Holmes H; Lancina MG; He W; Lee BP; Frost MC; Rajachar RM In Inducible nitric oxide releasing poly-(ethylene glycol)-fibrinogen adhesive hydrogels for tissue regeneration, MRS Proceedings, Cambridge Univ Press: 2013; pp 39–44.
3. Sierra DH, Fibrin sealant adhesive systems: a review of their chemistry, material properties and clinical applications. Journal of Biomaterials Applications 1993, 7 (4), 309–352. [PubMed: 8473984]
4. Brown AC; Barker TH, Fibrin-based biomaterials: modulation of macroscopic properties through rational design at the molecular level. Acta biomaterialia 2014, 10 (4), 1502–1514.10.1016/j.actbio.2013.09.008. [PubMed: 24056097]
5. Piechocka IK; Bacabac RG; Potters M; Mackintosh FC; Koenderink GH, Structural hierarchy governs fibrin gel mechanics. Biophys J 2010, 98 (10), 2281–9.10.1016/j.bpj.2010.01.040. [PubMed: 20483337]
6. Linnes MP; Ratner BD; Giachelli CM, A fibrinogen-based precision microporous scaffold for tissue engineering. Biomaterials 2007, 28 (35), 5298–306.10.1016/j.biomaterials.2007.08.020. [PubMed: 17765302]
7. Hadjipanayi E; Kuhn P-H; Moog P; Bauer A-T; Kuekrek H; Mirzoyan L; Hummel A; Kirchhoff K; Salgin B; Isenburg S, The fibrin matrix regulates angiogenic responses within the hemostatic microenvironment through biochemical control. PloS one 2015, 10 (8), e0135618. [PubMed: 26317771]
8. Martino MM; Briquez PS; Ranga A; Lutolf MP; Hubbell JA, Heparin-binding domain of fibrin (ogen) binds growth factors and promotes tissue repair when incorporated within a synthetic matrix. Proceedings of the National Academy of Sciences 2013, 110 (12), 4563–4568.10.1073/pnas.1221602110.
9. Lutolf M; Hubbell J, Synthetic biomaterials as instructive extracellular microenvironments for morphogenesis in tissue engineering. Nature biotechnology 2005, 23 (1), 47–55.10.1038/nbt1055.
10. Osathanon T; Linnes ML; Rajachar RM; Ratner BD; Somerman MJ; Giachelli CM, Microporous nanofibrous fibrin-based scaffolds for bone tissue engineering. Biomaterials 2008, 29 (30), 4091–9.10.1016/j.biomaterials.2008.06.030. [PubMed: 18640716]
11. Isenberg JS; Ridnour LA; Espey MG; Wink DA; Roberts DD, Nitric oxide in wound-healing. Microsurgery 2005, 25 (5), 442–51.10.1002/micr.20168. [PubMed: 16044466]
12. Sabanai K; Tsutsui M; Sakai A; Nakamura T; Shimokawa H; Yanagihara N, [Biochemical markers of bone turnover. New aspect. Nitric oxide synthase and bone metabolism]. Clinical calcium 2009, 19 (8), 1133–1141.CliCa090811331141. [PubMed: 19638697]
13. Hetrick EM; Shin JH; Paul HS; Schoenfisch MH, Anti-biofilm efficacy of nitric oxide-releasing silica nanoparticles. Biomaterials 2009, 30 (14), 2782–9.10.1016/j.biomaterials.2009.01.052. [PubMed: 19233464]
14. Li Y; Lee PI, Controlled nitric oxide delivery platform based on S-nitrosothiol conjugated interpolymer complexes for diabetic wound healing. Molecular pharmaceutics 2010, 7 (1), 254–266.10.1021/mp900237f. [PubMed: 20030413]
15. Cooke JP; Losordo DW, Nitric oxide and angiogenesis. Circulation 2002, 105 (18), 2133–2135.10.1161/01.CIR.0000014928.45119.73. [PubMed: 11994243]

16. Murrell GA, Using nitric oxide to treat tendinopathy. British journal of sports medicine 2007, 41 (4), 227–231.10.1136/bjsm.2006.034447. [PubMed: 17289859]
17. Inoue A; Hiruma Y; Hirose S; Yamaguchi A; Hagiwara H, Reciprocal regulation by cyclic nucleotides of the differentiation of rat osteoblast-like cells and mineralization of nodules. Biochemical and biophysical research communications 1995, 215 (3), 1104–1110.10.1006/bbrc.1995.2577. [PubMed: 7488037]
18. Van'T Hof RJ; Ralston SH, Nitric oxide and bone. Immunology 2001, 103 (3), 255–261.10.1046/j.1365-2567.2001.01261.x. [PubMed: 11454054]
19. Ridnour LA; Windhausen AN; Isenberg JS; Yeung N; Thomas DD; Vitek MP; Roberts DD; Wink DA, Nitric oxide regulates matrix metalloproteinase-9 activity by guanylyl-cyclase-dependent and-independent pathways. Proceedings of the National Academy of Sciences 2007, 104 (43), 16898–16903.10.1073/pnas.0702761104.
20. Hou Y; Janczuk A; Wang P, Current trends in the development of nitric oxide donors. Current pharmaceutical design 1999, 5 (6), 417–442. [PubMed: 10390607]
21. Armour KJ; Armour KE; Van't Hof RJ; Reid DM; Wei XQ; Liew FY; Ralston SH, Activation of the inducible nitric oxide synthase pathway contributes to inflammation-induced osteoporosis by suppressing bone formation and causing osteoblast apoptosis. Arthritis & Rheumatism 2001, 44 (12), 2790–2796. [PubMed: 11762939]
22. Szomor ZL; Appleyard RC; Murrell GA, Overexpression of nitric oxide synthases in tendon overuse. Journal of orthopaedic research 2006, 24 (1), 80–86.10.1002/jor.20009. [PubMed: 16419972]
23. Lin J; Wang M-X; Wei A; Zhu W; Murrell G, The cell specific temporal expression of nitric oxide synthase isoforms during Achilles tendon healing. Inflammation Research 2001, 50 (10), 515–522.10.1007/PL00000228. [PubMed: 11713906]
24. Zhang C; Biggs TD; Devarie-Baez NO; Shuang S; Dong C; Xian M, S-Nitrosothiols: chemistry and reactions. Chemical Communications 2017, 53 (82), 11266–11277.10.1039/c7cc06574d. [PubMed: 28944382]
25. Frost MC; Meyerhoff ME, Controlled photoinitiated release of nitric oxide from polymer films containing S-nitroso-N-acetyl-DL-penicillamine derivatized fumed silica filler. Journal of the American Chemical Society 2004, 126 (5), 1348–1349.10.1021/ja039466i. [PubMed: 14759186]
26. Seliktar D, Designing Cell-Compatible Hydrogels for Biomedical Applications. Science 2012, 336 (6085), 1124–1128. [PubMed: 22654050]
27. Iwata H; Matsuda S; Mitsuhashi K; Itoh E; Ikada Y, A novel surgical glue composed of gelatin and N-hydroxysuccinimide activated poly (L-glutamic acid):: Part 1. Synthesis of activated poly (L-glutamic acid) and its gelation with gelatin. Biomaterials 1998, 19 (20), 1869–1876.10.1016/S0142-9612(98)00095-7. [PubMed: 9855188]
28. Noailly J; Van Oosterwyck H; Wilson W; Quinn TM; Ito K, A poroviscoelastic description of fibrin gels. Journal of biomechanics 2008, 41 (15), 3265–3269.10.1016/j.jbiomech.2008.09.002. [PubMed: 18930461]
29. Magatti D; Molteni M; Cardinali B; Rocco M; Ferri F, Modeling of fibrin gels based on confocal microscopy and light-scattering data. Biophysical journal 2013, 104 (5), 1151–1159.10.1016/j.bpj.2013.01.024. [PubMed: 23473498]
30. Bouten PJ; Zonjee M; Bender J; Yauw ST; van Goor H; van Hest JC; Hoogenboom R, The chemistry of tissue adhesive materials. Progress in Polymer Science 2014, 39 (7), 1375–1405.10.1016/j.progpolymsci.2014.02.001.
31. McCarthy CW; Goldman J; Frost MC, Synthesis and Characterization of the Novel Nitric Oxide (NO) Donating Compound, S-nitroso-N-acetyl-D-penicillamine Derivatized Cyclam (SNAP-Cyclam). ACS applied materials & interfaces 2016, 8 (9), 5898–5905.10.1021/acsami.5b12548. [PubMed: 26859235]
32. McCarthy CW; Guillory RJ; Goldman J; Frost MC, Transition-Metal-Mediated Release of Nitric Oxide (No) from S-Nitroso-N-Acetyl-D-Penicillamine (SNAP): Potential Applications for Endogenous Release of No at the Surface of Stents Via Corrosion Products. ACS applied materials & interfaces 2016, 8 (16), 10128–10135.10.1021/acsami.6b00145. [PubMed: 27031652]

33. Field L; Dilts RV; Ravichandran R; Lenhert PG; Carnahan GE, An unusually stable thionitrite from N-acetyl-D, L-penicillamine; X-ray crystal and molecular structure of 2-(acetylamino)-2-carboxy-1, 1-dimethylethyl thionitrite. Journal of the Chemical Society, Chemical Communications 1978, (6), 249–250.
34. Devore JL, Probability and Statistics for Engineering and the Sciences. 4th ed.; Wadsworth Publishing Company: 1995; p 169.
35. International A, Standard Test Method for Strength Properties of Tissue Adhesives in Lap-Shear by Tension Loading In ASTM F2255–05, West Conshohocken, PA, 2010.
36. Li Y; Meng H; Liu Y; Narkar A; Lee BP, Gelatin microgel incorporated poly (ethylene glycol)-based bioadhesive with enhanced adhesive property and bioactivity. ACS applied materials & interfaces 2016, 8 (19), 11980–11989.10.1021/acsami.6b01364. [PubMed: 27111631]
37. Freiberg S; Zhu X, Polymer microspheres for controlled drug release. International journal of pharmaceutics 2004, 282 (1), 1–18.10.1016/j.ijpharm.2004.04.013. [PubMed: 15336378]
38. Zhu W; Wang B; Zhang Y; Ding J, Preparation of a thermosensitive and biodegradable microgel via polymerization of macromonomers based on diacrylated Pluronic/oligoester copolymers. European polymer journal 2005, 41 (9), 2161–2170.10.1016/j.eurpolymj.2005.04.006.
39. Sung B; Kim C; Kim M-H, Biodegradable colloidal microgels with tunable thermosensitive volume phase transitions for controllable drug delivery. Journal of colloid and interface science 2015, 450, 26–33.10.1016/j.jcis.2015.02.068. [PubMed: 25797395]
40. Riccio DA; Schoenfisch MH, Nitric oxide release: Part I. Macromolecular scaffolds. Chemical Society Reviews 2012, 41 (10), 3731–3741.10.1039/c2cs15272j. [PubMed: 22362355]
41. Caruso EB; Petralia S; Conoci S; Giuffrida S; Sortino S, Photodelivery of nitric oxide from water-soluble platinum nanoparticles. Journal of the American Chemical Society 2007, 129 (3), 480–481.10.1021/ja067568d. [PubMed: 17226997]
42. Batchelor MM; Reoma SL; Fleser PS; Nuthakki VK; Callahan RE; Shanley CJ; Politis JK; Elmore J; Merz SI; Meyerhoff ME, More lipophilic dialkyldiamine-based diazeniumdiolates: synthesis, characterization, and application in preparing thromboresistant nitric oxide release polymeric coatings. Journal of medicinal chemistry 2003, 46 (24), 5153–5161.10.1021/jm030286t. [PubMed: 14613318]
43. Frost MC; Reynolds MM; Meyerhoff ME, Polymers incorporating nitric oxide releasing/generating substances for improved biocompatibility of blood-contacting medical devices. Biomaterials 2005, 26 (14), 1685–1693.10.1016/j.biomaterials.2004.06.006. [PubMed: 15576142]
44. Carpenter AW; Schoenfisch MH, Nitric oxide release: Part II. Therapeutic applications. Chemical Society Reviews 2012, 41 (10), 3742–3752.10.1039/c2cs15273h. [PubMed: 22362384]
45. Wink DA; Hines HB; Cheng RY; Switzer CH; Flores-Santana W; Vitek MP; Ridnour LA; Colton CA, Nitric oxide and redox mechanisms in the immune response. Journal of leukocyte biology 2011, 89 (6), 873–891.10.1189/jlb.1010550. [PubMed: 21233414]
46. Thomas DD; Espey MG; Ridnour LA; Hofseth LJ; Mancardi D; Harris CC; Wink DA, Hypoxic inducible factor 1α, extracellular signal-regulated kinase, and p53 are regulated by distinct threshold concentrations of nitric oxide. Proceedings of the National Academy of Sciences of the United States of America 2004, 101 (24), 8894–8899.10.1073/pnas.0400453101. [PubMed: 15178764]
47. Schanuel FS; Santos KSR; Monte-Alto-Costa A; de Oliveira MG, Combined nitric oxide-releasing poly (vinyl alcohol) film/F127 hydrogel for accelerating wound healing. Colloids and Surfaces B: Biointerfaces 2015, 130, 182–191.10.1016/j.colsurfb.2015.04.007. [PubMed: 25907598]
48. Yao X; Liu Y; Gao J; Yang L; Mao D; Stefanitsch C; Li Y; Zhang J; Ou L; Kong D, Nitric oxide releasing hydrogel enhances the therapeutic efficacy of mesenchymal stem cells for myocardial infarction. Biomaterials 2015, 60, 130–140.10.1016/j.biomaterials.2015.04.046. [PubMed: 25988728]
49. Davis ME; Gumucio JP; Sugg KB; Bedi A; Mendias CL, MMP inhibition as a potential method to augment the healing of skeletal muscle and tendon extracellular matrix. Journal of Applied Physiology 2013, 115 (6), 884–891.10.1152/japplphysiol.00137.2013. [PubMed: 23640595]
50. Lin TW; Cardenas L; Soslowsky LJ, Biomechanics of tendon injury and repair. Journal of biomechanics 2004, 37 (6), 865–877.10.1016/j.jbiomech.2003.11.005. [PubMed: 15111074]

51. Skelton S; Bostwick M; O'Connor K; Konst S; Casey S; Lee BP, Biomimetic adhesive containing nanocomposite hydrogel with enhanced materials properties. Soft Matter 2013, 9 (14), 3825–3833.10.1039/c3sm27352k.

52. Strehin I; Nahas Z; Arora K; Nguyen T; Elisseeff J, A versatile pH sensitive chondroitin sulfate–PEG tissue adhesive and hydrogel. Biomaterials 2010, 31 (10), 2788–2797.10.1016/j.biomaterials.2009.12.033. [PubMed: 20047758]

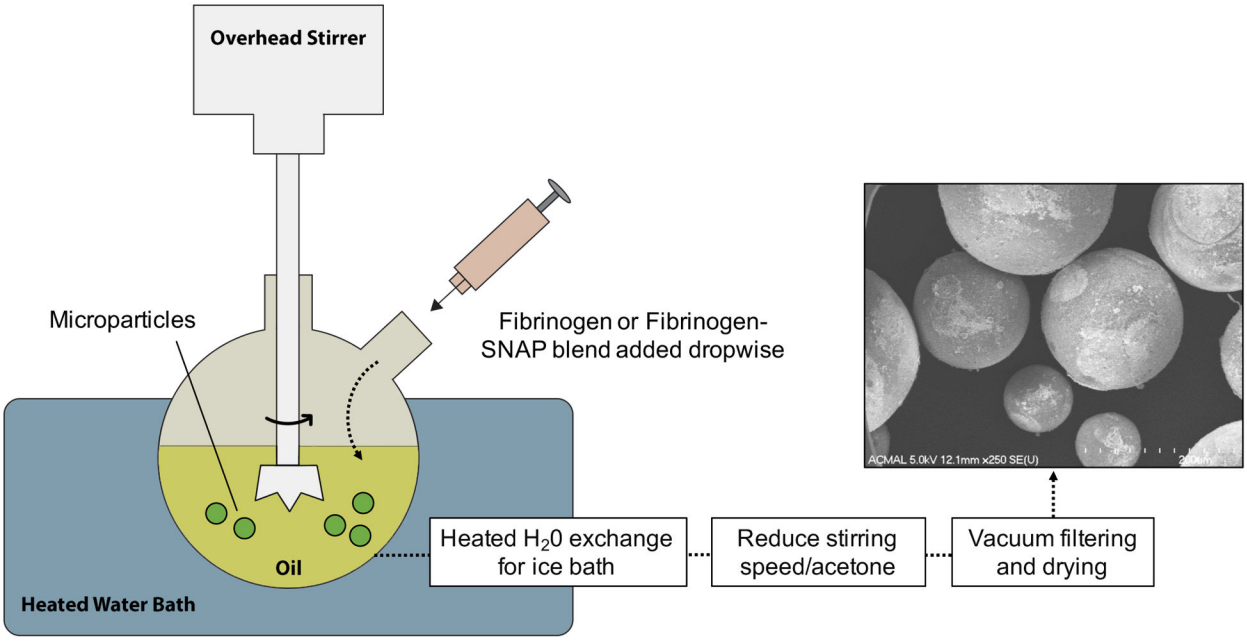

Figure 1. Microparticle Synthesis.

Set up for generating microparticles in varying diameters using emulsion polymerization. Three rotational stirring speeds (750, 1000, and 1500 rpm) generated three different particle sizes (R1, R2, and R3 respectively).

A)

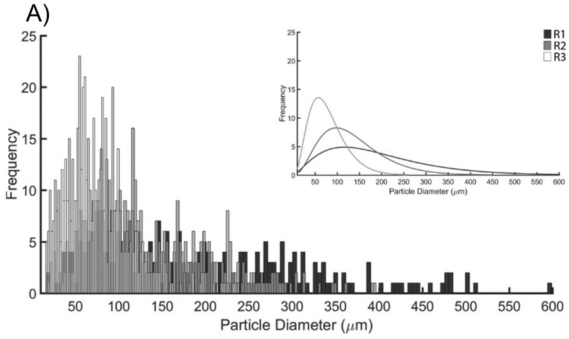

B)

	Particle Characteristics		γ Distribution Parameters		95% Confidence Intervals	
RPM	Mean Diameter (μm)	Standard Error of Mean	α	β	Lower	Upper
750 (R1)	193	7.48	2.52	76.8	2.14 2.96	64.1 91.9
1,000 (R2)	135	3.44	3.64	37.2	3.20 4.14	32.4 42.7
1,500 (R3)	78.8	1.73	3.73	21.2	3.35 4.15	18.9 23.7

Figure 2. Microparticle characterization.

A) Distribution histograms of particle diameters based on the rotational speed at which they were formed (R1: 750 rpm, R2: 1000 rpm, R3: 1500 rpm). Inset: Gamma distribution fit of the respective histograms showing relative particle size distributions. B) Summary of mean diameter, standard error of the mean, gamma distribution parameters, and 95% ($p \leq 0.05$) confidence intervals for the associated gamma distribution parameters. Mean particle diameter decreases with increased stirring speed. Gamma distribution parameters highlight increasing uniformity in particle distributions as stirring speed is increased.

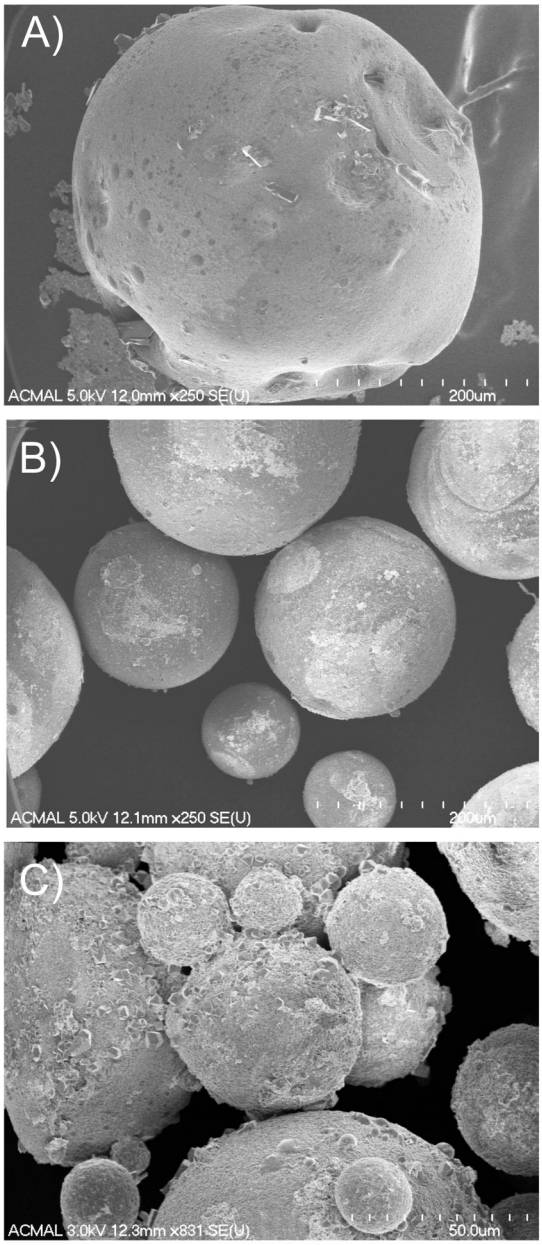

Figure 3. FESEM images of microparticles formed at three distinct stirring speeds.

A) R1: 750 rpm, B) R2: 1000 rpm, and C) R3: 1500 rpm. R2 particles are spherical, exhibit minimal debris and are similar in size. Conversely, R1 and R3 particles exhibit clumping, debris, and irregular shape. In A and B, scale bar = 200 μm, in C scale bar = 50 μm.

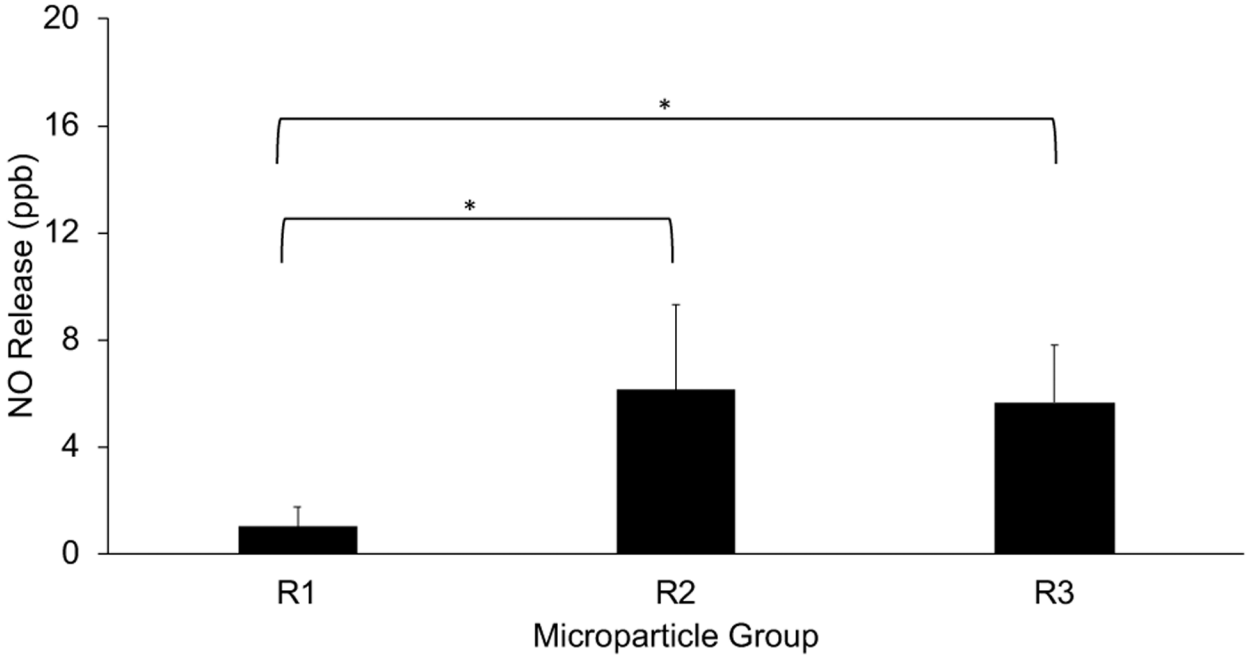

Figure 4. Photolytic NO release from microparticles.

Average photolytic (light induced, 470nm LED at 0.4V, 0.6V, 0.8V, 1V, 0.8V, 0.6V, 0.4V for 5 minutes at each voltage) nitric oxide release from isolated R1, R2, and R3 microparticles (5mg). Smaller diameter particles (R2, R3) exhibit significantly higher NO release compared to larger particles (R1). (R1: 750 rpm, R2: 1000 rpm, R3: 1500 rpm). * statistically significant ($p<0.05$) differences.

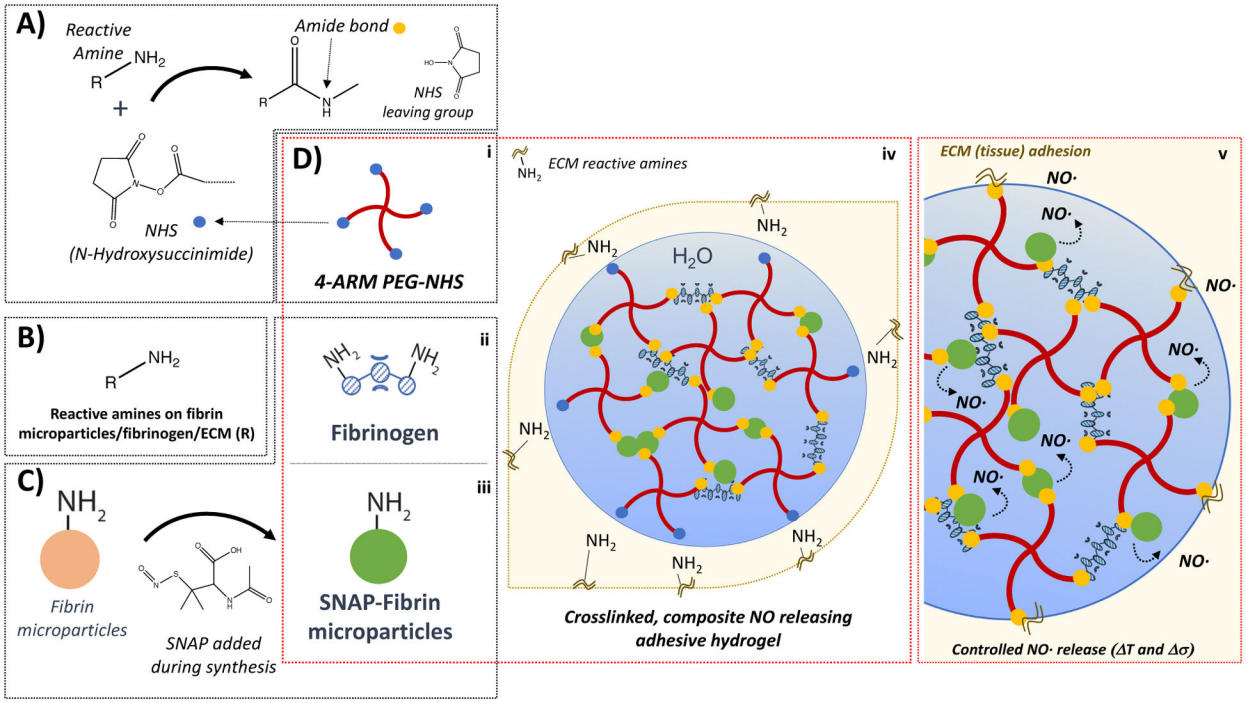

Figure 5. Composite hydrogel reactive groups, synthesis, and function.

A) NHS crosslinking chemistry in PEG-NHS forming stable conjugate (amide bond) with reactive amines; B) reactive amines also present in fibrinogen (D-ii), fibrin particles (D-iii); C) synthesis of SNAP-Fibrin microparticles; D) (i-iii) elements of composite adhesive hydrogel; (iv) curing hydrogel in-situ; (v) fully cured hydrogel including tissue adhesion and controlled NO release.

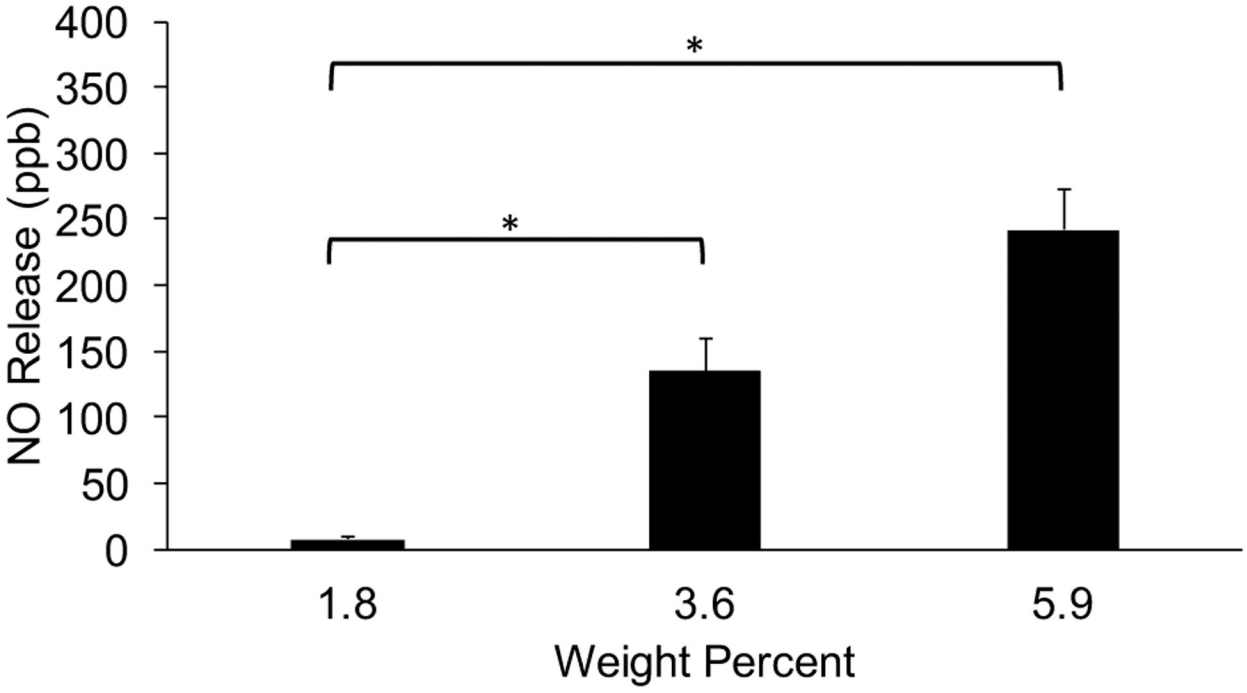

Figure 6A. Photolytic NO release from composite hydrogels.

PEG-NHS-Fgn-R2-SNAP hydrogels were prepared with Fgn-R2-SNAP microparticles at three weight percentages (1.8, 3.6 and 5.9) were exposed to a controlled light source. Release behavior was directly related to the weight percent of incorporated particles. * statistically significant ($p<0.05$) differences.

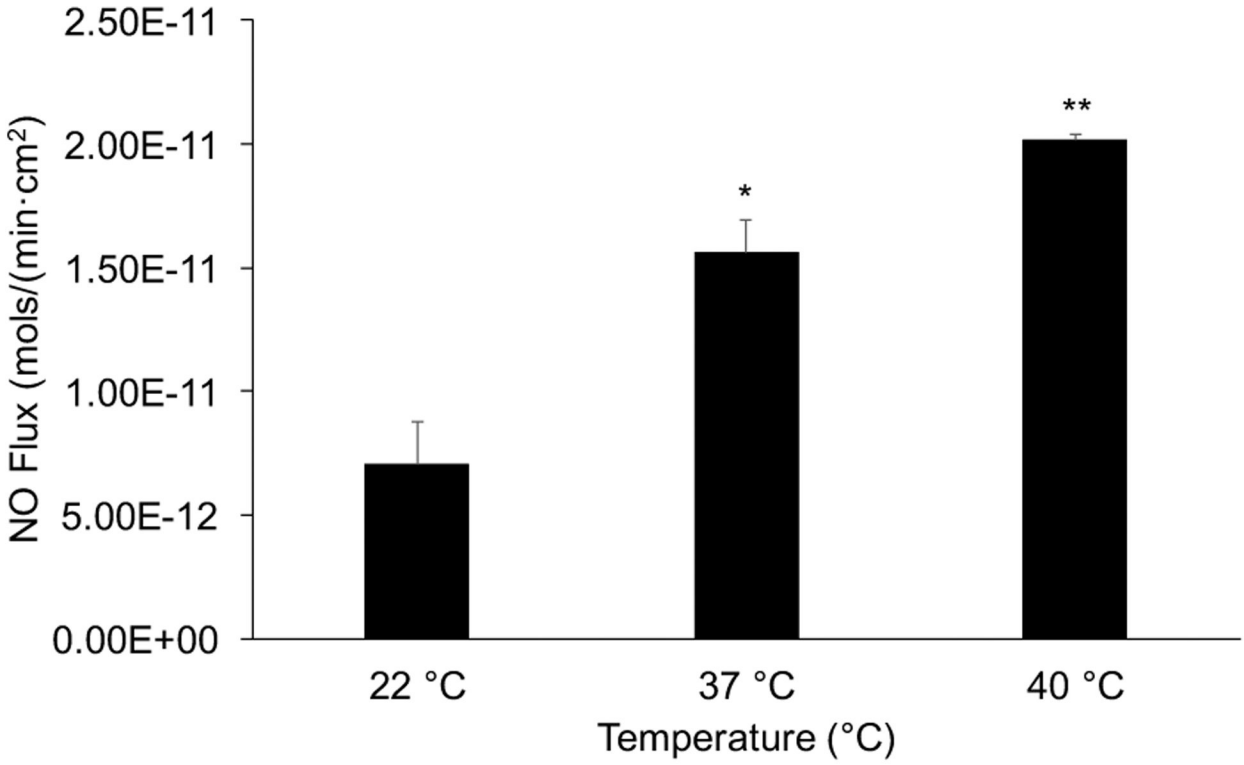

Figure 6B. Thermally induced NO release from composite hydrogels.

NO releasing composite hydrogels (PEG-NHS-Fgn-R2-SNAP with 5.9 wt % Fgn-R2-SNAP microparticles) displayed temperature controlled NO release. Body temperature (37 °C) stimulated a significant increase in NO flux compared to room temperature (22°C) controls (*$p < 0.05$), while the release at the clinical limit for thermal treatment (40°C) was significantly higher than both room and body temperature (**$p<0.05$).

A)

	Swelling Ratio	Water Content	Degradation (Days)
Control (PEG-NHS-Fgn)	20.36 ± 1.79	95.1% ± 0.4%	29.5 ± 1.00
Composite (PEG-NHS-Fgn-R2)	17.27 ± 0.96*	94.2% ± 0.3%*	31.6 ± 3.77

B)

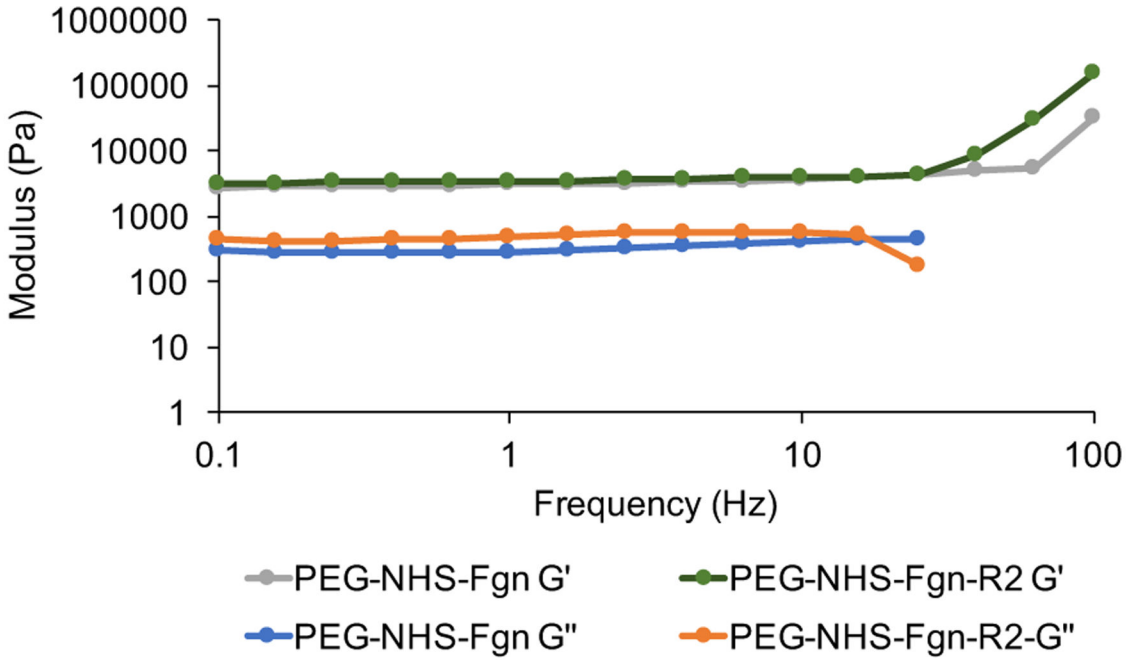

Figure 7. Physical properties of composite hydrogels.

A) The swelling ratio and water content of composite hydrogels (PEG-NHS-Fgn-R2, 5.9wt % microparticles) was found to be significantly lower than controls (PEG-NHS-Fgn), indicative of increased cross-linking in microparticle-composites. B) The viscoelastic behavior of PEG-NHS-Fgn-R2 composites (5.9wt% R2 microparticles) was compared to controls using standard plate rheometry and subjecting hydrogels to oscillatory strain at a frequency of 0.1–100 Hz. Composites showed no significant change in storage modulus but a significant increase in loss modulus compared to controls. The elevated G" reveals an increased viscous dissipation ability of the composite. The reversible physical bond existing in the structure can be sacrificed before the breaking of chemical bond during the energy dissipation compared to controls.

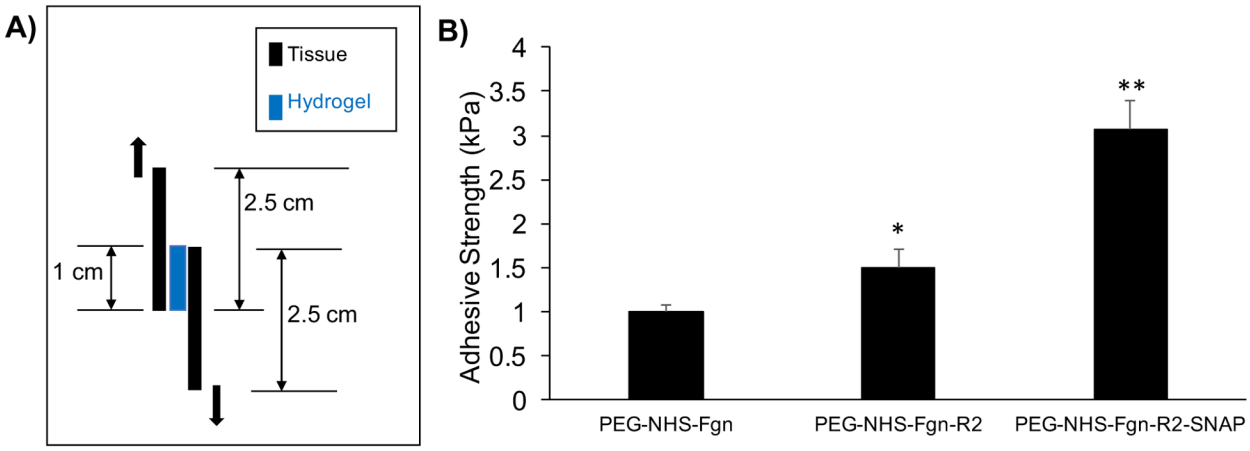

Figure 8. Tissue adhesivity of composite hydrogels.

A) Lap shear experimental set up. B) Both fibrin only (PEG-NHS-Fgn-R2) and SNAP fibrin (PEG-NHS-Fgn-R2-SNAP) composites exhibited significantly higher tissue adhesivity than controls (*$p<0.05$). Additionally, SNAP fibrin composites exhibited significantly higher tissue adhesivity than fibrin only composites (**$p<0.05$). This suggests that the hydrogel matrix can be stabilized by the addition of fibrin particles alone as well as the NO free radical.

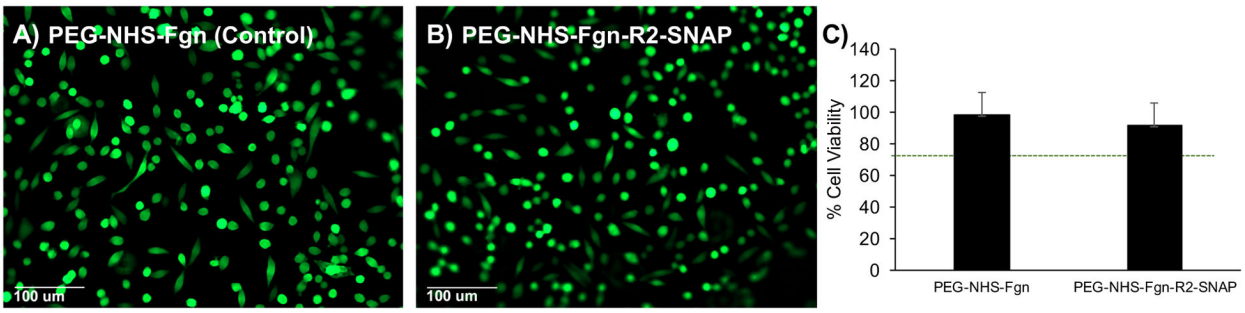

Figure 9. Cell adhesion and viability.

A) Control PEG-NHS-Fgn hydrogels and B) PEG-NHS-Fgn-R2-SNAP composite hydrogels sustained cell adhesion, morphology, and viability in culture indicated by calcein-AM (live-green) and ethidium bromide (dead-red) staining. C) Relative cell viability measured through the MTT assay complimented Live/Dead results, indicating the non-cytotoxicity of both hydrogel formulations, where cell viabilities greater than 70% were considered non-cytotoxic. The MTT Cell Proliferation Assay measures the cell proliferation rate, when changes in cellular metabolism lead to apoptosis or necrosis, this results in a reduction in cell viability.